Struct Multidisc Optim (2016) 54:45–61
DOI 10.1007/s00158-015-1385-y

RESEARCH PAPER

Multi-objective crashworthiness optimization of perforated square tubes using modified NSGAII and MOPSO

Abolfazl Khalkhali[1] · **Majid Mostafapour**[1] · **Seyed Mohamad Tabatabaie**[1] · **Behnam Ansari**[1]

Received: 8 March 2015 / Revised: 30 November 2015 / Accepted: 5 December 2015 / Published online: 13 January 2016

Abstract In this paper, multi-objective optimization of perforated square tubes is performed considering absorbed energy, peak crushing force and weight of the tube as three conflicting objective functions. In the multi-objective optimization problem (MOP), absorbed energy and peak crushing force are defined by polynomial models extracted using the software GEvoM based on the train and test data obtained from the numerical simulation of quasi-static crushing of the perforated square tubes using ABAQUS. To verify the numerical procedure, 16 different experimental tests are performed and then the experimental and numerical results are compared together. The comparison shows reasonable similarities between the numerical and experimental results. The MOP is solved using modified Non-dominated Sorting Genetic Algorithm II (NSGAII) and Multi-objective Particle Swarm Optimization (MOPSO) and then the solutions are combined for non-dominated sorting to obtain the non-dominated individuals of 3-objective optimization. 105 optimum points are extracted from the multi-objective optimization process. Finally, Nearest to Ideal Point (NIP) method and Technique for Ordering Preferences by Similarity to Ideal Solution (TOPSIS) method are employed to find trade-off optimum design points out of all non-dominated individuals compromising all three objective functions together.

Keywords Perforated square tube · Quasi-static crushing · ABAQUS · GEvoM · Modified NSGAII · MOPSO · TOPSIS

✉ Abolfazl Khalkhali
ab_khalkhali@iust.ac.ir

[1] Automotive simulation and optimal design research laboratory, School of Automotive Engineering, Iran University of Science and Technology, Tehran, Iran

1 Introduction

Investigating different methods of absorbing released energy to reduce damages and injuries is one of important research areas, which has received considerable attention over the past decades (Johnson 1972; Johnson and Reid 1978; Jones and Wierzbicki 1983; Guoxing 2003). Thin walled structures which are capable of sustaining prescribed loads and dissipating energies while undergoing plastic deformation are widely used in different industries such as automotive, aerospace and marine industries as energy absorbing structures (Bartczak et al. 2010). Engineering structures are often perforated for various reasons such as weight reduction, assembling the equipment and drainage paint (in painting process), dirt and water as drain hole. Another important role of the holes which is specific in energy absorbing components is the role of crash initiating (Mamalis et al. 2009). Embodying geometrical discontinuities can affect the axial collapse mode, by ensuring a stable collapse process and decreasing the initial peak load (Mamalis et al. 2009).

Crushing behavior of perforated tubes has been studied experimentally and numerically by various investigators in previous works. Arnold and Altenh (2004) performed quasi-static compressive testing of extruded aluminum alloy square tube specimens with and without the presence of dual centrally located circular hole discontinuities. They showed that the presence of the circular discontinuity within some of the tubes slightly degraded the crush force efficiency. Chenga et al. (2006) conducted experimental investigation to compare the crush characteristics of aluminum alloy extrusions with centrally located through-hole discontinuities. They showed that the peak crush load was reduced by incorporating the through-hole crush initiators within a range of 5.2–18.7 %, and total energy absorption was increased within a range of 26.6–74.6 %. Mamalis et al. (2009) performed finite element (FE) simulation of square steel tubes with circular

discontinuities subjected to quasi-static axial loadings using the LS-DYNA explicit FE code. They found good agreement between the results of the numerical model and testing results from the axial loading.

All of the previous works show that there are set of holes configuration which could provide optimum crashworthiness characteristic. But, a general study on the optimal holes configuration has not been done in the previous works. Optimum energy absorbing structures must have high energy absorbing capability, low weight and low peak crushing force, simultaneously (Khakhali et al. 2010a). Thus optimization of such structures is a multi-objective optimization problem (MOP) (Arora 2012). Energy absorption and peak crushing force, as two objective functions of this 3-objective optimization problem, cannot be calculated using analytical formulas in many of such problems. Therefore, to approximate these two objective functions, an appropriate surrogate model can be used based on experimental or numerical results. To perform multi-objective optimization under such circumstance, a combination of numerical simulation, artificial neural network modeling and modified NSGAII algorithm has been used successfully by some of the authors previously (Khakhali et al. 2010b; Khalkhali and Safikhani 2012; Khalkhali et al. 2011; Amanifard et al. 2008a). In such studies, training GMDH neural network using input–output data obtained from numerical simulation gives polynomial models that can be used as objective function in multi-objective optimization process.

Evolutionary algorithms have been widely used for multi-objective optimization because of their natural properties suited for these types of problems. Therefore, most of the difficulties and deficiencies within the classical methods in solving multi-objective optimization problems are eliminated (Arora 2012). Non-dominated Sorting Genetic Algorithm (NSGA-II) proposed by Srinivas and Deb for solving MOPs (Srinivas and Deb 1994; Collette and Siarry 2003) is one of the most powerful evolutionary algorithms for solving multi-objective optimization problems. To improve NSGA-II, Nariman-Zadeh proposed modified NSGA-II which use ε-elimination algorithm instead of crowding factor (Nariman-Zadeh et al. 2006). The Modified NSGA-II has been used successfully in the previous works (Khakhali et al. 2010b, 2011; Khalkhali and Safikhani 2012).

Particle Swarm Optimization (PSO) which was introduced by Kennedy and Eberhart (1995) is a numerical search algorithm that is used to find parameters that minimize a given objective, or *fitness* function (Kennedy and Eberhart 1995). PSO is a robust stochastic optimization algorithm based on the intelligence and movement of swarms where the concept of social interaction to problem solving is applied (Ebbesen et al. 2012). PSO has gained significant popularity due to its attractive structure and high performance over the past few years (Kennedy and Eberhart 1995). It uses a number of agents (particles) that constitute a swarm moving around in the search space looking for the optimized answer. Each particle is treated as a point in a search space which adapts its "flying" according to its own flying experience as well as the flying experience of other particles. Each particle keeps track of its coordinates in the search space which are associated with the best solution (fitness) that has achieved so far by that particle. This value is called personal best, *Pbest*. Another best value that is tracked by the PSO is the best value gained so far by any particle in the adjacent of that particle, which is called *Gbest*.

In the multi-objective problems where the objectives conflict with each other, there is no single optimal solution as the best with respect to all the objective functions. Instead, there is a set of optimal solutions, known as Pareto optimal solutions or non-dominated optimum points (Fonseca and Fleming 1993; Coello Coello and Christiansen 2000; Coello Coello et al. 2002; Pareto 1896). For a MOP with more number of objective functions the number of non-dominated optimum points is often more than that for another MOP with the lower number of objective function. Different evolutionary algorithms with different fundamental natures may neglect some of optimum points. Therefore, combination of different evolutionary methods for multi-objective optimization could provide better finding of all non-dominated optimum points. In this way, combination of modified NSGAII and multi-objective particle swarm optimization (MOPSO) as two powerful multi-objective optimization techniques can be employed.

In this paper, quasi-static crushing behavior of the thin-walled square tubes with geometrical discontinuities in the form of circular holes under quasi static load is studied experimentally and numerically. Experimental tests were carried out to validate the numerical model which was performed using commercial software ABAQUS/Explicit. Using experimentally verified FE model, 96 different finite element analyses are then performed to obtain the training and testing data for developing the polynomial models using GEvoM software. To find optimal configuration of holes and thereby improve crashworthiness characteristic of the tube, developed polynomials are then used in a multi-objective optimization process considering absorbed energy, peak crushing force and weight of the tube as three conflicting objectives. To solve this MOP, NSGA-II and MOPSO are used and then the solutions are combined for non-dominated sorting to obtain the optimum individuals. After finding out the non-dominated points, two different trade-off optimum points are obtained using NIP and TOPSIS methods.

2 Experimental procedure

Schematic view of the perforated square tubes is shown in Fig. 1, where w, L, D and t denote width of the tube, length of the tube, holes diameter, and thickness of the tube, respectively. According to Fig. 1, four different sides of the square

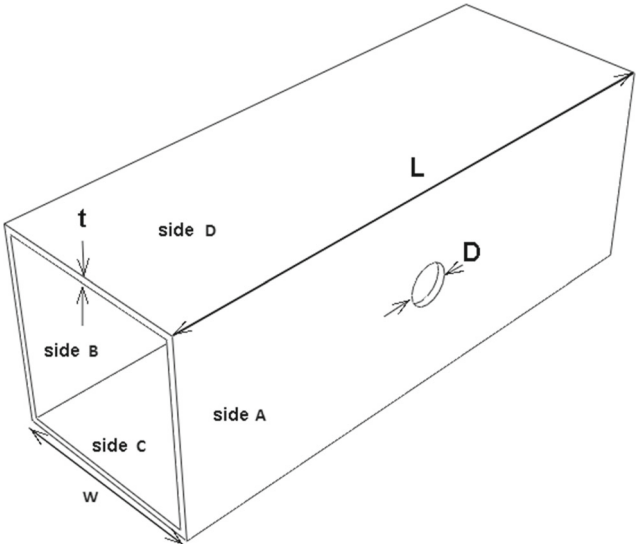

Fig. 1 Schematic view of the perforated square tubes

All specimens were prepared from mild steel. For reducing the residual stresses, stress relief heat treatment was carried out. Specimens were heated to 1020 °C which is less than transformation temperature and held at this temperature for 2 h and then gradually returned to the room temperature. One standard tensile specimen was also constructed to determine the mechanical properties of the constitutive material. The same heat treatment was done equally on this tensile specimen. Stress–strain curve of the constitutive material obtained from the tensile test is depicted in Fig. 3.

The quasi-static crushing tests on the perforated square tubes were performed using SANTAM testing machine STM-150 series with a prescribed cross-head speed of 5 mm/min. Data from the load cell and extensometer was acquired using a computer controlled data acquisition system. Results of the quasi static crushing experiments of perforated square tubes will be used for validation of numerical simulation in the next section.

tube are named by the latters A, B, C and D. With respect to these four sides, four different types of specimens are considered: Type A which the holes are located on the side A, Type B which the holes are located on the sides A and B, Type C which the holes are located on the sides A and C, Type D which the holes are located on all sides. In the experimental tests, total tube length (L), width of the tubes (w), wall thickness (t) and holes diameter (D) were considered constant and equal to 200 mm, 70 mm, 15 mm, and 1.5 mm, respectively. Equal distances are considered between the holes which can be calculated from L/ (n + 1) where n represent number of holes on each side (see Fig. 2). Different specimens with different holes location and holes number can now be considered. Table 1 shows 16 different specimens evaluated experimentally in the present work.

3 Quasi-static finite element analysis

Quasi-static axial crushing of perforated square tubes was modeled using ABAQUS/Explicit. Behavior of the material was considered according to the curve depicted in Fig. 3 which shows the stress–strain curve obtained from the tensile test. The post-yield material response was defined using 49 points from the stress–strain curve. The testing machine base and movable crosshead were modeled using two rigid surface located on the bottom and top of the tube. Medial axis algorithm in ABAQUS mesh control was used to qualify mesh around the holes. To simulate interactions between the model surfaces, General Contact with the friction coefficient of 0.3 was used. Velocity was applied to the tube via the top rigid surface. The loading rate applied in actual quasi-static

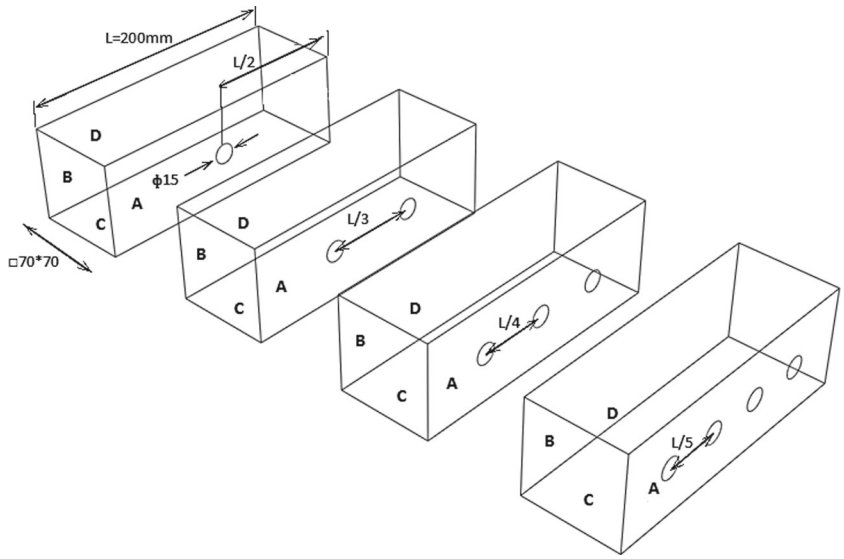

Fig. 2 Distances between holes for specimens of the type A with $n = 1, 2, 3$ and 4

Table 1 Different specimens evaluated using experimental tests

Type	Specimen No.	Perforated side	Hole location	Number of holes on each side (n)	Total number of holes
A	A1	A	L/2	1	1
	A2	A	L/3	2	2
	A3	A	L/4	3	3
	A4	A	L/5	4	4
B	B1	A,B	L/2	1	2
	B2	A,B	L/3	2	4
	B3	A,B	L/4	3	6
	B4	A,B	L/5	4	8
C	C1	A,C	L/2	1	2
	C2	A,C	L/3	2	4
	C3	A,C	L/4	3	6
	C4	A,C	L/5	4	8
D	D1	A,B,C,D	L/2	1	4
	D2	A,B,C,D	L/3	2	8
	D3	A,B,C,D	L/4	3	12
	D4	A,B,C,D	L/5	4	16

experiments, 5 mm/min for performing experiments in this work, was too slow that increased the time step too much. In order to reduce the time step of the analysis, the velocity of the rigid surface was artificially speeded up to 0.115 m/s. Moreover, it was needed to apply loading as smooth as possible because sudden movements cause stress waves which can induce noisy or inaccurate solution. In a typical smooth loading curve, initial velocity and initial slope of the curve, which is equal to initial acceleration, are zero. This ensures that loading takes place gradually and unnecessary dynamic effects will be avoided. In this way, the applied velocity was controlled using the AMPLITUDE option and the SMOOTH STEP sub option was used in ABAQUSE/Explicit to ensure an accurate quasi-static analysis (Khakhali et al. 2011).

After a FE analysis if the simulation is quasi-static, the velocity of the material is very small and accordingly inertial forces are negligible. Therefore, in this situation, internal energy is nearly equal to the work applied by the external forces while the kinetic energy is small and should not exceed a small fraction of internal energy. In the present work, comparison of the internal and kinetic energy for all specimens shows that kinetic energy is very small compared to the internal energy and therefore the numerical simulation can be considered as a quasi-static analysis, confidently.

Figures 4, 5 and 6 show the experimental and numerical deformed shapes for some specimens at the cross-head displacement of 30, 100 and 150 mm, respectively. The figures show close similarity between the numerical and experimental simulation results. The comparison of the numerical and experimental force-displacement responses for some of the specimens are also shown in Fig. 7. There is reasonable similarity between the results obtained from the numerical analysis and the experimental load deflection responses. Absorbed energies and peak crushing forces obtained from the numerical and experimental analysis are also represented in Table 2 for some of the test specimens. One possible reason for some degree of difference between the experimental and the numerical load deflection responses could be attributed to non-homogeneous material properties in the test specimens. Also the geometrical imperfections due to the forming process can cause some reduction in the value of peak load. These results confidently indicate the validity of the numerical analysis.

Such verified FE model can be employed now to generate input–output data to train and test the GMDH model using GEvoM software. Considering schematic view of the test specimens shown in Fig. 1, various designs can be generated by changing the holes diameter, the holes number and the holes location. For each type of the tubes, four levels including

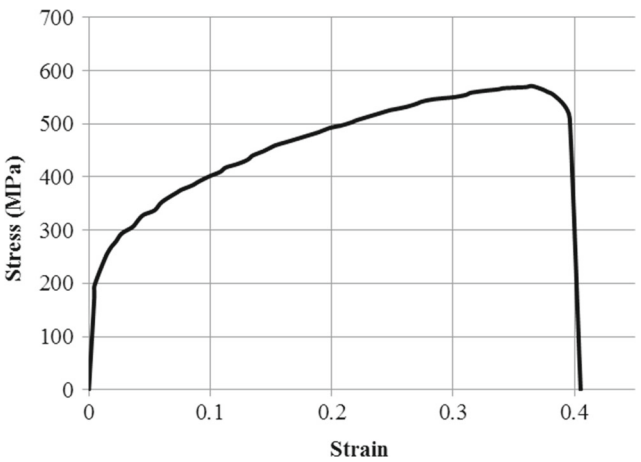

Fig. 3 Stress–strain curve for constitutive material of the specimens

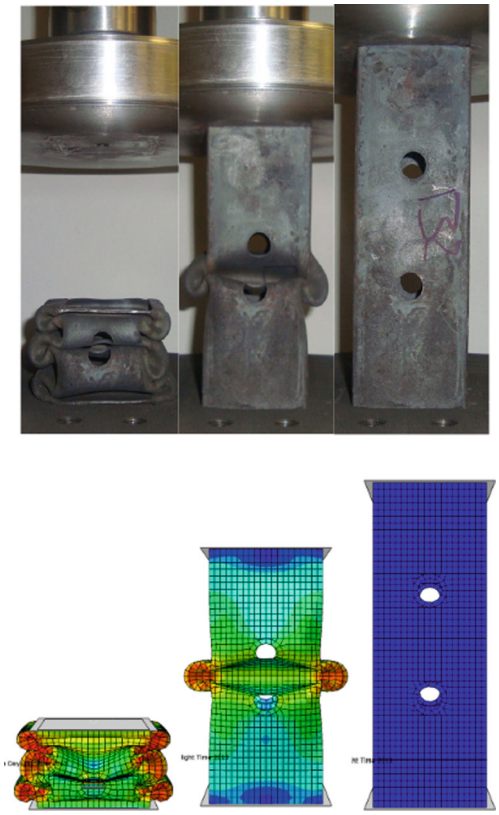

Fig. 4 Comparison of experimental and numerical shape of deformation for specimen B2

1, 2, 3, and 4 holes have been considered for the holes number and 6 levels including 5, 15, 25, 35, 45 and 55 mm have been also considered for the holes diameter. Therefore, if the number of the cases is considered uniform, using factorial design of experiments there will be 24 different combinations of the holes number and diameter. All these combinations have been modeled and their peak crushing force and absorbed energy have been determined. Considering four different types of specimens (A, B, C and D) a data table of 96 different designs of square tubes with circular holes is developed and then evaluated by the finite element method using ABAQUS software. Some of the simulation results are given Table 3.

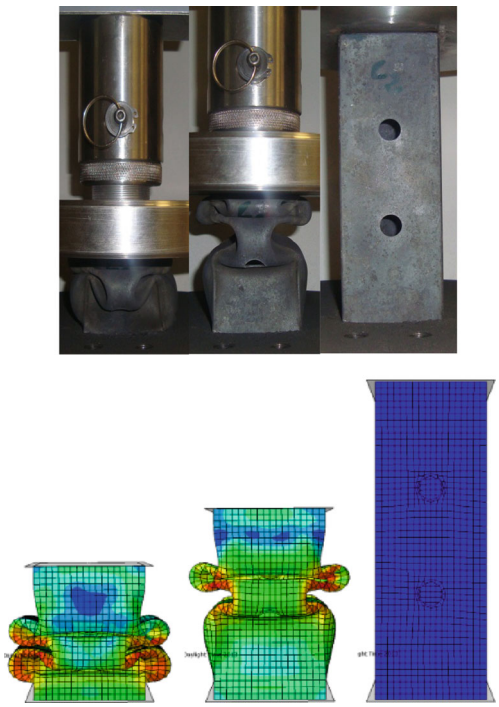

Fig. 5 Comparison of experimental and numerical shape of deformation for specimen C2

4 Modeling using GEvoM

By means of GMDH algorithm a model can be represented as set of neurons in which different pairs of them in each layer are connected through a quadratic polynomial and thus produce new neurons in the next layer. Such representation can be used in modeling to map inputs to outputs. The formal definition of the identification problem is to find a function $\hat{f}$ so that can be approximately used instead of actual one, f in order to predict output $\hat{y}$ for a given input vector $X=(x_1, x_2, x_3, \ldots, x_n)$ as close as possible to its actual output y.

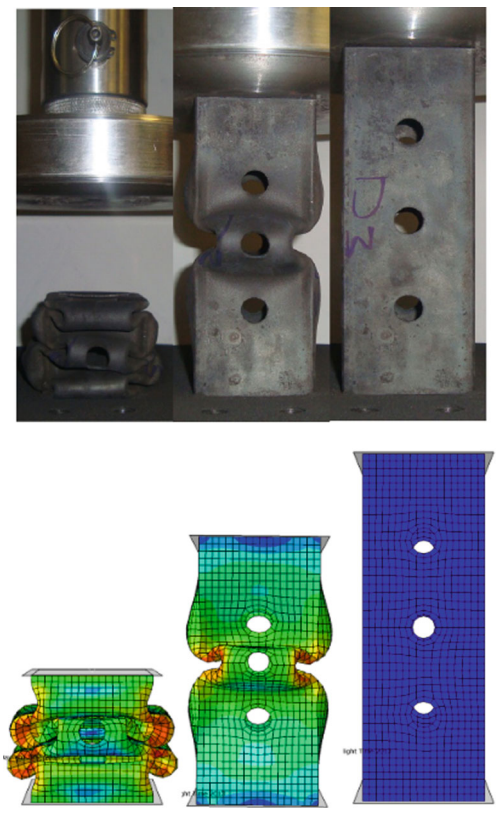

Fig. 6 Comparison of experimental and numerical shape of deformation for specimen D3

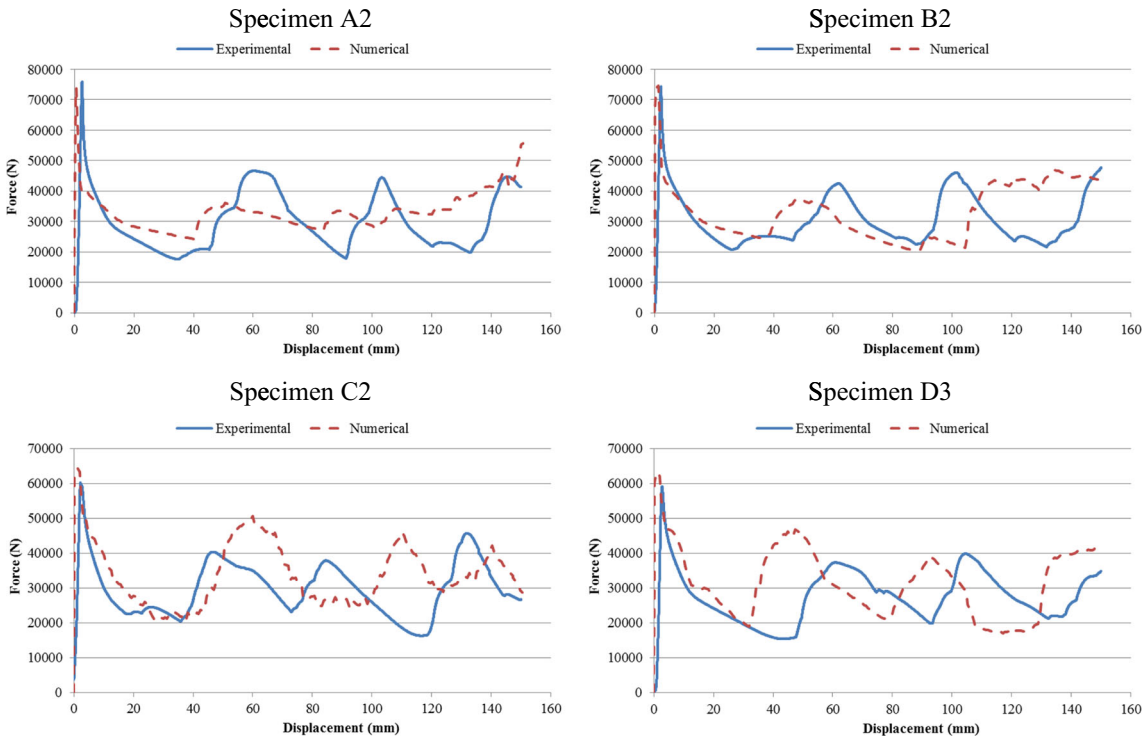

Fig. 7 Comparison of experimental and numerical Force-displacement diagram for specimens A2, B2, C2 and D3

General connection between inputs and output variables can be expressed by a complicated discrete form of the Volterra functional series in the form of

$$\hat{y} = a_0 + \sum_{i=1}^{n} a_i x_i + \sum_{i=1}^{n}\sum_{j=1}^{n} a_{ij} x_i x_j + \sum_{i=1}^{n}\sum_{j=1}^{n}\sum_{i=1}^{n} a_{ijk} x_i x_j x_k + \ldots, \quad (1)$$

where is known as the Kolmogorov-Gabor polynomial (Ivakhnenko 1971; Liu and Kadirkamanathan 1999). This full form of mathematical description can be represented by a system of partial quadratic polynomials consisting of only two neurons in the form of

$$\hat{y} = G(x_i, x_j) = a_0 + a_1 x_i + a_2 x_j + a_3 x_i x_j + a_4 {x_i}^2 + a_5 {x_j}^2. \quad (2)$$

Table 2 Absorbed energies and peak crushing forces obtained from numerical and experimental analysis for some of test specimens

Specimen No.	Peak crushing force (KN)		Absorbed energy (J)	
	Numerical	Experimental	Numerical	Experimental
A1	70	71	4402.3	4220.8
A2	78.7	75.8	4328	4691.8
A4	75.7	70.7	3903.2	4373.5
B1	78.7	71.2	4574.4	4633
B3	72.6	69.8	4363	4446.6
B4	73.8	68.6	4289.1	4393.5
C2	64.2	60.1	5092.9	4871.9
D3	63.3	59.1	4747.4	4437.5

Polynomial coefficient values and network connectivity configuration are two important points in the design of GMDH-type neural networks. Some works by Nariman-zadeh et al. (Amanifard et al. 2008a; Amanifard et al. 2008b; Atashkari et al. 2007; Tavoli et al. 2006) represent the deployment of genetic algorithm (GA) and singular value decomposition (SVD) simultaneously for optimal design of both connectivity configuration and the values of embodied polynomial coefficient, respectively. This methodology was developed as a software named GEvoM (http://research.guilan.ac.ir/gevom). In fact, GEvoM is a program that generates polynomials based on GMDH-type neural networks to model any kind of input–output data.

The input–output data pairs used in the present work involve the data tables obtained from the numerical modeling represented in Section 3. Such results are separated in four different data tables according to different type of the tubes (A, B, C and D). Number of the holes and holes diameters are considered as inputs whilst the absorbed energy (E) and the peak crushing force (F_{max})

Table 3 Some of the input–output data employed in GEvoM and their GMDH responses

Specimen type	Number of holes	Diameter of holes (mm)	Absorbed energy (J)		Peak crushing force (kN)	
			FEM	GMDH	FEM	GMDH
A	4	5	4525.06	4370	78700	79864
A	2	20	4095.79	4270	74800	73968
A	4	25	4044.54	4230	73400	74372
A	1	45	4203.65	4090	66500	65132
A	3	45	3848.66	3740	64400	66493
B	2	15	4214.24	4120	74500	72311.04
B	3	25	4097.69	4200	64700	65119.52
B	2	35	4080.96	4020	59100	59804.99
B	1	45	4445.50	4520	59400	60753.38
B	2	45	3866.93	4030	53700	54784.19
C	4	15	5202.89	4930	77100	73573.05
C	2	25	4610.80	4750	67400	65777.06
C	3	35	4537.34	4680	60300	60915.71
C	1	45	4938.75	4740	54900	53601.17
C	2	45	4794.88	4660	55600	53962.23
D	3	5	5069.65	5180	78400	79770.57
D	1	15	6148.43	6290	79600	76797.48
D	1	25	5472.50	5770	62000	61173.54
D	3	35	4264.29	4140	48200	45791.94
D	2	45	3972.07	4160	47500	48902.83

are considered as outputs. Each data table consists of the total 24 patterns which have been obtained from the finite element analysis to train and test such GMDH–type neural networks. However, in order to demonstrate the prediction ability of evolved GMDH-type neural networks, the data have been divided into two different sets, namely, training and testing sets. The training set consists of 19 out of 24 input–output data pairs and the testing set also consists of 5 unforeseen inputs-output data samples. In the evolutionary method sub option of GEvoM a population of 30 individuals with a crossover probability (Pc) of 0.7 and mutation probability (Pm) of 0.07 has been used in 400 generations in which no further improvement has been achieved for such population size. Some of the input–output data employed in GEvoM and their GMDH responses are depicted in Table 3.

The good ability of GMDH-type neural network models for modeling and prediction of the numerically obtained energy absorption data are depicted in Fig. 8 both for training and testing data of type A,B,C,D. Such behaviors have also been shown for peak crushing force both for training and testing data of type A, B, C and D in Fig. 9. It is evident from these figures that the evolved GMDH-type neural network in terms of simple polynomial equations can successfully model and predict the output of the testing data that has not been used during the training process. The corresponding polynomial representation for absorbed energy and peak crushing force of type A, B, C and D are given in Appendix A. The goodness of fit of the obtained GEvoM models was also measured using Mean Absolute Percentage Error (MAPE) as a statistical metric (see Table 4). It is very evident that the model fits well the set of observations.

5 Methods to find the trade-off optimum point

After multi-objective optimization it is desired to choose the trade-off optimal design point through the all non-dominated individuals. Two methods which are used in the present work are introduced in this section.

5.1 Nearest to ideal point (NIP method)

In the nearest to ideal point method, first, an ideal point with the best values of each objective function is

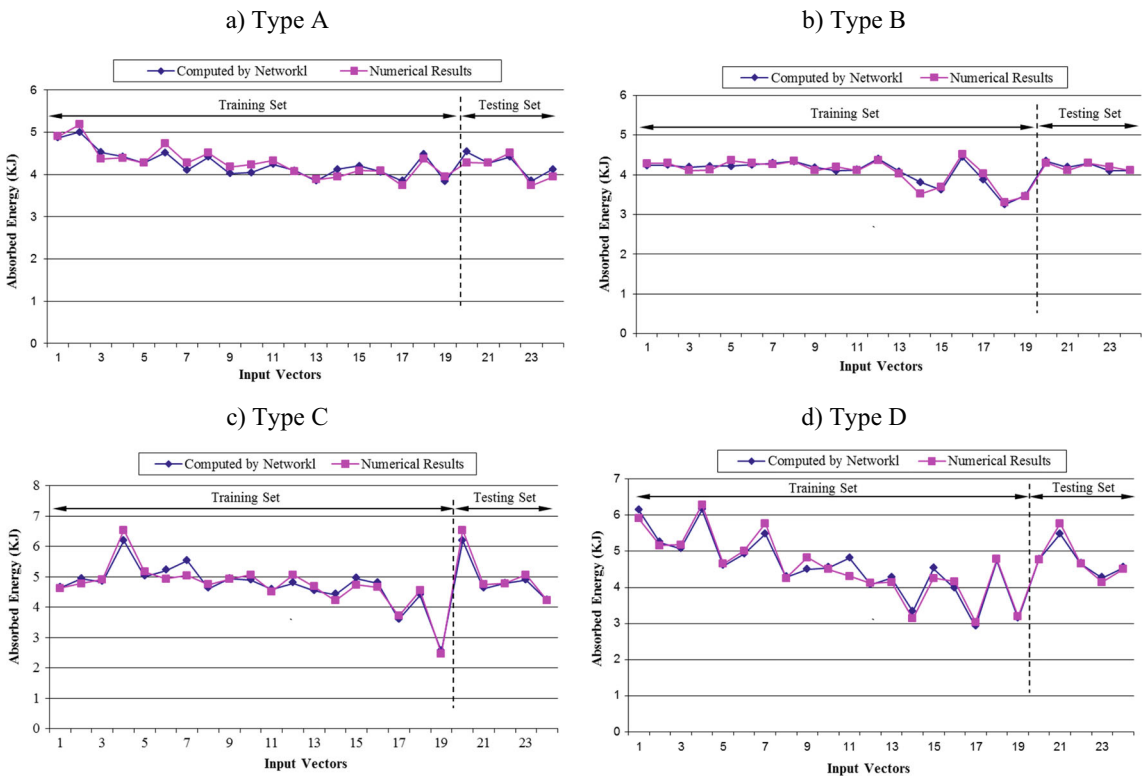

Fig. 8 Variations of the absorbed energy (E) of types A to D with input data

considered. Secondly, the distances between all non-dominated points and the ideal point are calculated. Finally, the desired point represents minimum distance to the ideal point.

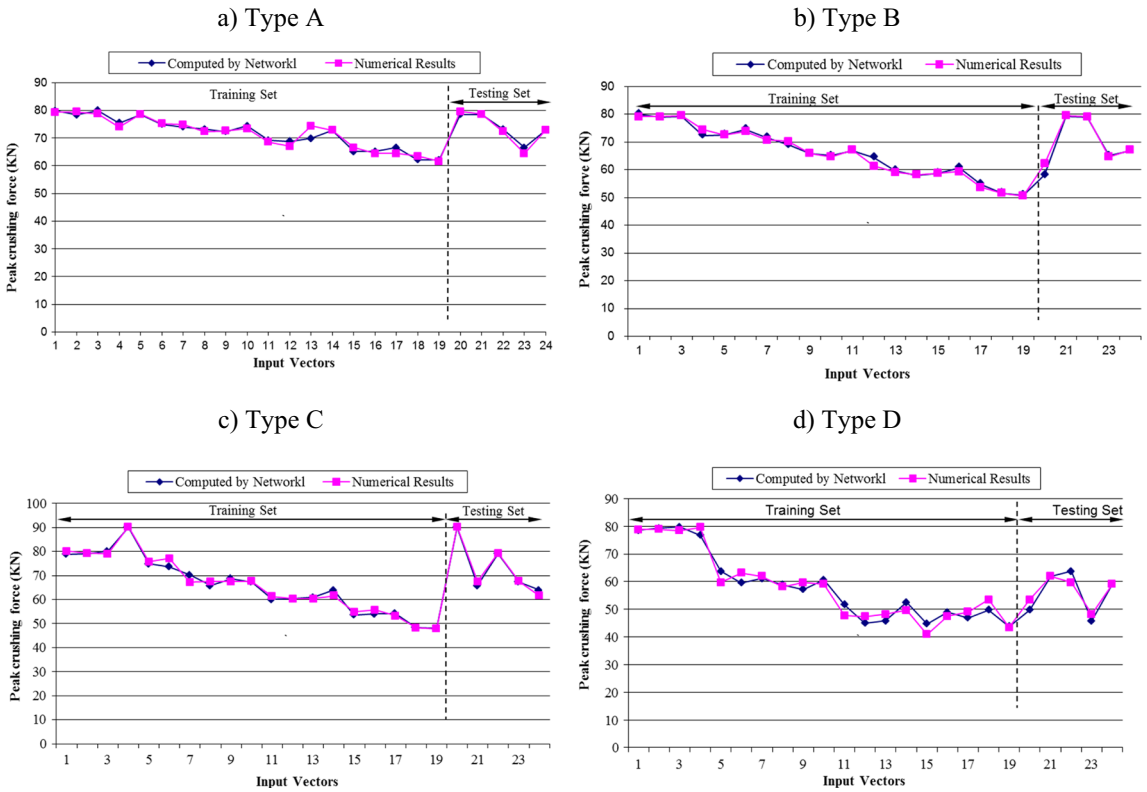

Fig. 9 Variations of the peak crushing force (F_{max}) of type A to D with input data

Table 4 Mean absolute percentage error list for GEvoM models

Type	MAPE			
	Training set		Testing set	
	Absorbed energy	Peak crushing force	Absorbed energy	Peak crushing force
A	0.98 %	0.56 %	2.90 %	1.53 %
B	0.60 %	1.50 %	1.88 %	1.39 %
C	1 %	0.58 %	3.50 %	1.72 %
D	1 %	1.22 %	3.43 %	3.62 %

5.2 Technique for order performance by similarity to ideal solution (TOPSIS method)

TOPSIS method is able to apply a weight or an importance factor to each objective function and propose a point according to these importance factors. The method consists of several steps. Initially, the values of objective functions (S) and weight of each objective (W) must be specified. S_{ij} denotes the ith optimum point of the jth objective function. W_j represents the weight of jth objective function which must satisfy the following equation:

$$\sum_{j=1}^{2} W_j = 1 \tag{3}$$

In the second step, values of S_{ij} matrix will be normalized based on the next equation:

$$S = \frac{S_{ij}}{\sqrt{\sum_{i=1}^{r} S_{ij}^2}} \quad \text{for j} = 1,2 \quad \text{i} = 1,2,3,\ldots,\tau \tag{4}$$

And $\hat{S}$ matrix will be formed as follows:

$$\check{S} = [\widetilde{S_{11}}, \widetilde{S_{12}} : \widetilde{S_{21}}, \widetilde{S_{22}} : \ldots : \widetilde{S_{\tau 1}}, \widetilde{S_{\tau 2}}] \tag{5}$$

In the third step, elements of the normalized matrix will be multiplied by related weight factors:

$$\widehat{S_{\iota J}} = W_j \times \widetilde{S_{\iota J}} \tag{6}$$

The normalized weight matrix will be appeared as the following equation:

$$\hat{S} = \left[\widehat{S_{11}}, \widehat{S_{12}} : \widehat{S_{21}}, \widehat{S_{22}} : \ldots : \widehat{S_{\tau 1}}, \widehat{S_{\tau 2}}\right] \tag{7}$$

In the fourth round, values of S^+ and S^- will be found according to the following equations:

$$S^+ = \left(\min\left(\widehat{S_{11}}, \widehat{S_{21}}, \ldots, \widehat{S_{\tau 1}}\right), \min\left(\widehat{S_{12}}, \widehat{S_{22}}, \ldots, \widehat{S_{\tau 2}}\right)\right) \tag{8}$$

$$S^- = \left(\max\left(\widehat{S_{11}}, \widehat{S_{21}}, \ldots, \widehat{S_{\tau 1}}\right), \max\left(\widehat{S_{12}}, \widehat{S_{22}}, \ldots, \widehat{S_{\tau 2}}\right)\right) \tag{9}$$

In the fifth step, the separation measures h_i^+ and h_i^- for each Pareto point will be found using the following equations:

$$h_i^+ = \sqrt{\sum_{j=1}^{2} \left(\widehat{S_{lJ}} - S_j^+\right)^2} \quad \text{for i} = 1,2,3,\ldots,\tau \tag{10}$$

$$h_i^- = \sqrt{\sum_{j=1}^{2} \left(\widehat{S_{lJ}} - S_j^-\right)^2} \quad \text{for i} = 1,2,3,\ldots,\tau \tag{11}$$

In the sixth step, H_i which represents the relative accuracy, will be calculated for each Pareto curve:

$$H_i = \frac{h_i^-}{h_i^+ - h_i} \quad 0 \le H_i \le 1 \tag{12}$$

In the final step, maximum value of H_i will be selected and the objective functions' values and corresponding optimum design variables will be determined based on the selected value of H.

6 Multi-objective crashworthiness optimization of the square tubes

In the present work, to improve the crashworthiness characteristics of perforated square tubes, a multi-objective optimization problem (MOP) has been defined and solved considering absorbed energy (E), peak crushing force (F_{max}) and weight of the tube (W) as three conflicting objectives. The polynomial neural network models obtained in previous sections are now deployed in the three-objective optimization problem which can be formulated in the following form:

$$\begin{cases} Maximize & E = f_1(T,n,D) & (Absorbed\ Energy) \\ Minimize & W = f_2(T,n,D) & (Weight\ of\ the\ Tube) \\ Minimize & F_{\max} = f_3(T,n,D) & (Peak\ Crushing\ Force) \\ Design\ Variable\ Bounds: & & \\ & T \in \{A, B, C, D\} & \\ & n \in \{1, 2, 3, 4\} & \\ & 5mm \le D \le D_{max} & \end{cases} \tag{13}$$

Due to the geometrical restriction between holes diameter and length of the tube, D_{max} which is the upper bound of the

holes diameter in equation (13) is considered 35 mm for $n=4$, 45 mm for $n=3$ and 55 mm for both $n=2$ and $n=1$. To solve the above multi-objective optimization problem, the modified NSGAII (Khalkhali and Safikhani 2012) and MOPSO were used and consequently two separate sets of optimal solutions were obtained. All optimum points obtained from both methods were combined together and then non-dominated sorting procedure, which takes all of populations as input and then returns the first non-dominated front as output, was performed. After non-dominated sorting, some of the points found by modified NSGAII and also some of the points found by MOPSO were eliminated. The remained set of optimum points which is the respond of the MOP is called re-fronted optimum points.

MOPSO approach which was first proposed by Coello et al. (2004) is based on the traditional particle swarm optimization (PSO). In this approach, to solve the multi-objective optimization problems, Pareto dominance is incorporated into PSO algorithm. MOPSO also uses a constraint-handling mechanism and a special mutation operator that considerably improves the exploratory capabilities of this algorithm. Main algorithm of MOPSO is summarized as:

1. The population POP is initialized.
2. The speed of each particle is initialized.
3. Each of the particles in POP is evaluated.
4. The positions of the particles are stored, which represent non-dominated vectors in the repository REP.
5. Hypercubes of the search space explored so far are generated, and the particles are located using these hypercubes as a coordinate system, where each particle's coordinates are defined according to the values of its objective functions.
6. The memory of each particle is initialized.

$$PBESTS_i = POP_i \tag{14}$$

7. WHILE maximum number of cycles has not been reached DO

a) The speed of each particle is computed using the following expression:

$$\boldsymbol{V}_i^{t+1} = \omega \boldsymbol{V}_i^t + C_1 r_1^t \left(\boldsymbol{PBESTS}_i - \boldsymbol{POP}_i^t\right) + C_2 r_2^t \left(\boldsymbol{REP}_m - \boldsymbol{POP}_i^t\right) \tag{15}$$

where V_i^t denotes velocity vector associated with *ith* particle in iteration t, $\mathrm{PBESTS_i}$ is the best position that the particle has had, $\mathrm{REP_m}$ is value of *mth* element of the repository, ω is the inertia weight of the particle introduced by Shi and Eberhart (1998). Inertia weight (ω) controls the trade-off between global (large ω) and local (small ω) experiences. Index m in $\mathrm{REP_m}$ is calculated using the hypercubes of the search space and performing roulette wheel (Coello et al. 2004). The algorithm uses two independent random numbers, r_1 and r_2 between 0 and 1. C_1 and C_2 are parameters which control the influence of the personal and global best particles.

In Equation (15) it is necessary to note to the definition of $\mathrm{PBESTS_i}$ because in multi-objective optimization, unlike single objective optimization, best position that the particle has had cannot be found simply. To solve a single objective optimization problem using PSO, best position of a particle is where that the cost function has minimum value (or maximum value for maximization problems) based on its travel history. In a multi-objective optimization problem, considering that multiple objective functions are supposed to be optimized simultaneously, a position may be considered a good position in the point of view of one objective function, while it may not be a good one in the point of view of the other objective function. Therefore in MOPSO for determining the $\mathrm{PBESTS_i}$ the concept of Pareto dominance is used. In this way, if in an increment the objective functions values for the *ith* particle dominate those contained in $\mathrm{PBESTS_i}$, the new value will be inserted in $\mathrm{PBESTS_i}$. Otherwise the $\mathrm{PBESTS_i}$ value for the *ith* particle remains unchanged. If neither of them is dominated by the other, then one of them will be selected randomly.

The value of V_i^t is clamped to the range $[V_{min}, V_{max}]$ to weaken the likelihood that the particle might leave the search space. Clerc and Kennedy showed that the constriction factor x as expressed in equation 16 and equation 17 may help to ensure convergence (Clerc and Kennedy 2002).

$$\boldsymbol{V}_i^{t+1} = x\left[\omega \boldsymbol{V}_i^t + C_1 r_1^t \left(\boldsymbol{PBESTS}_i - \boldsymbol{POP}_i^t\right) + C_2 r_2^t \left(\boldsymbol{REP}_m - \boldsymbol{POP}_i^t\right)\right] \tag{16}$$

$$x = \frac{2}{\left|2 - \phi - \sqrt{\phi^2 - 4}\right|} \quad \phi = C_1 + C_2 \;;\; \phi > 4 \tag{17}$$

b) Particles are moved to their new positions according to:

$$\boldsymbol{X}_i^{t+1} = \boldsymbol{X}_i^t + \boldsymbol{V}_i^{t+1} \tag{18}$$

where X_i^t *is* the current position of particle *i*.

c) The particles are maintained within the search space in case they go beyond their boundaries.

d) Each of the particles in POP is evaluated.

e) The contents of REP are updated together with the geographical representation of the particles within the hypercubes. This update consists of inserting all the currently non-dominated locations into the repository.

f) If the current position of the particle dominates the position in memory, the current position replaces the one in memory as follow:

$$PBESTS_i = POP_i \quad (19)$$

Otherwise the $PBESTS_i$ value is kept; if neither of the values is dominated by the other, then one of them can be selected randomly.

g) The loop counter is incremented.

8. End WHILE

The optimization parameters used in MOPSO are represented in Table 5.

In Fig. 10, all obtained optimum design points which are 105 points are shown in the 3D objective space. Figure 11 depicts the re-fronted non-dominated individuals of 3-objective optimization in the plane of (E-F_{max}), (E-W) and (F_{max}-W), separately. It should be noted that there is a single set of re-fronted individuals as a result of the 3-objective optimization of E, W and F_{max} that are shown in different planes together. In this figure, the remaining points from those obtained by modified NSGAII are shown by blue color and similarly the points remained from MOPSO are shown by red color.

It is clear that all of these optimum points are non-dominated and could be chosen by a designer. Evidently, choosing a better value for any objective function in the obtained non-dominated optimum points would cause a worse value for another objective. The corresponding design variables of these optimum points are the best possible design points. Hence, if any other set of design variables is chosen, the corresponding values of the pair of objectives will locate a point inferior to the obtained non-dominated optimum points.

It should be noted that the results of the three-objective optimization include results of the single objective optimization. The design point 'a' is the result of single objective optimization of absorbed energy. In fact, if a designer aims to maximize the absorbed energy, the design point 'a' which gives the best value of absorbed energy must be chosen. On the other hand, similarly, the design points 'b' and 'c' are the results of single objective optimization of weight and peak crushing force respectively. These optimum design points are shown in the Fig. 12 and the values of their design variables and objective functions are represented in Table 6. It is clear from Fig. 12 that the points 'a' and 'b' are almost located on two corners of the graph. It means that the optimum point with maximum absorbed energy has also maximum weight between all non-dominated individuals. On the other hand the optimum point with minimum weight has almost minimum absorbed energy between all non-dominated individuals too.

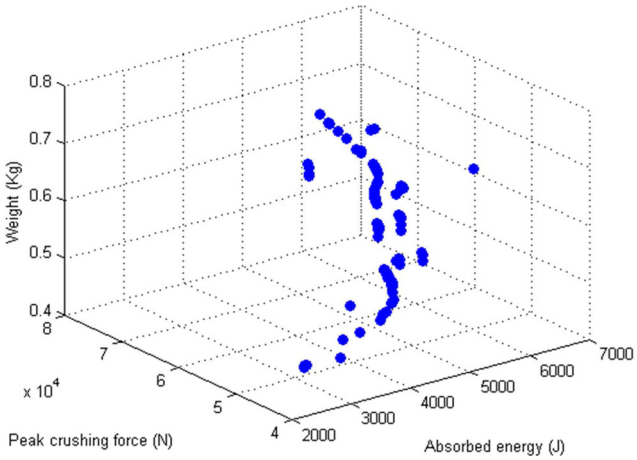

Fig. 10 Obtained refronted optimum points in the 3D objective space

It may be desired to find trade-off optimum design points out of all non-dominated individuals compromising all three objective functions. This can be achieved by two methods described in Section 5, namely, the Technique for Ordering Preferences by Similarity to Ideal Solution (TOPSIS) method and Nearest to Ideal Point (NIP) method. Consequently, trade-off optimum design points 'p' and 'q' are the points which have been obtained from the TOPSIS method and NIP method (considering equal weights for all objectives), respectively. In Fig. 12, on the planes of (E-W) and (F_{max}-W), both points 'p' and 'q' are non-dominated. But, on the plane of (E-F_{max}), it can be seen that point 'q' dominates point 'p'. Comparing locations of the optimum design points 'p' and 'q' on the planes show that from point 'p' to point 'q', energy absorption (E) and peak crushing force (F_{max}) improves about 39 % and 3 % respectively. However, another objective function, weight of the tube, is weakened about 36 %. Because increase in F_{max} from point 'q' to point 'p' is very low (about 3 %) and therefore it is negligible, the designer can choose one of these two points ('p' and 'q') by compromising between only two

Table 5 optimization parameters used in MOPSO

Common parameters	Magnitude
Swarm size	100 Particles
Iterations	250
C1, C2	2.05
ω	0.97
Mutation probability	0.05

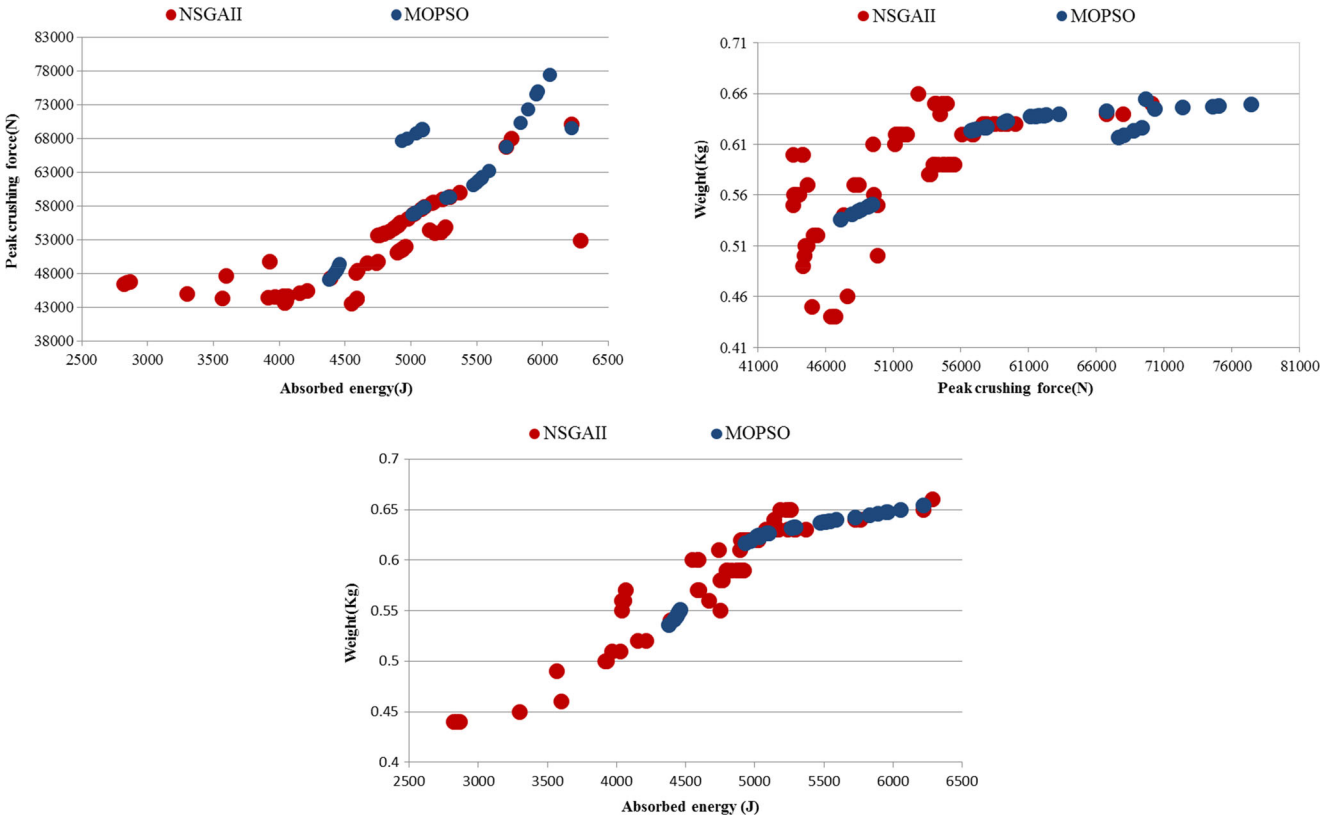

Fig. 11 Re-fronted optimum points in different planes, blue and red points were remained from the points obtained by modified NSGAII and MOPSO respectively

objective functions E and W. Values of design parameters and objective functions for the points 'p' and 'q' are represented in Table 6. It is noteworthy that the design point 'p' chosen by TOPSIS is the same as the point 'b' which is the answer of single objective optimization of W. Moreover, the value of its peak crushing force is very close to the point 'c' which is the answer of single objective optimization of F_{max}. It is clear that the optimum design points represented in Table 6 are some useful optimal design points which could not have been discovered without the use of the optimization process presented in this paper.

For comparison between the trade-off optimum design points, the point 'b' was chosen as the base line solution and the other solutions were compared with this optimum point by showing the percentage of increase or decrease on each objective. Such comparison results given in Table 6 contain interesting information and can help the designer to choose the best design point.

To investigate the effect of perforating the tubes on their energy absorption characteristics, a non-perforated sample has been modeled in ABAQUS/Explicit according to the conditions stated in Section 3 and its absorbed energy and peak crushing force have been determined numerically. The simulation results of the non-perforated sample have been compared with those of the trade-off optimum design points in Table 7. This comparison implies that, with neglecting the small reduction in the absorbed energy, at the optimum points the peak crushing force and weight of the perforated tubes have been remarkably improved compared to those of the non-perforated sample.

As another interesting obtained result which is shown in Fig. 12, 71 points from all of 105 non-dominated optimum design points (about 70 %) are from type D and the other remained points (about 30 %) are from Type C. It means that square tubes with more perforated sides dominate the other points. In fact, perforating the holes on the tubes considerably decreases weight of the tube and peak crushing force, which affects the dominance of the individuals significantly. However, the optimum design points of Type C also have interesting behavior. It can be seen from Fig. 12 that the values of all three objective functions in most of design points of Type C are moderate. It means that, from viewpoint of all objective functions, the design points of Type C exhibit moderate behavior. Design point 'r' can be simply recognized and chosen from the points of Type C. Its values of design variables and objective function are represented in Table 6. It can be seen from this table

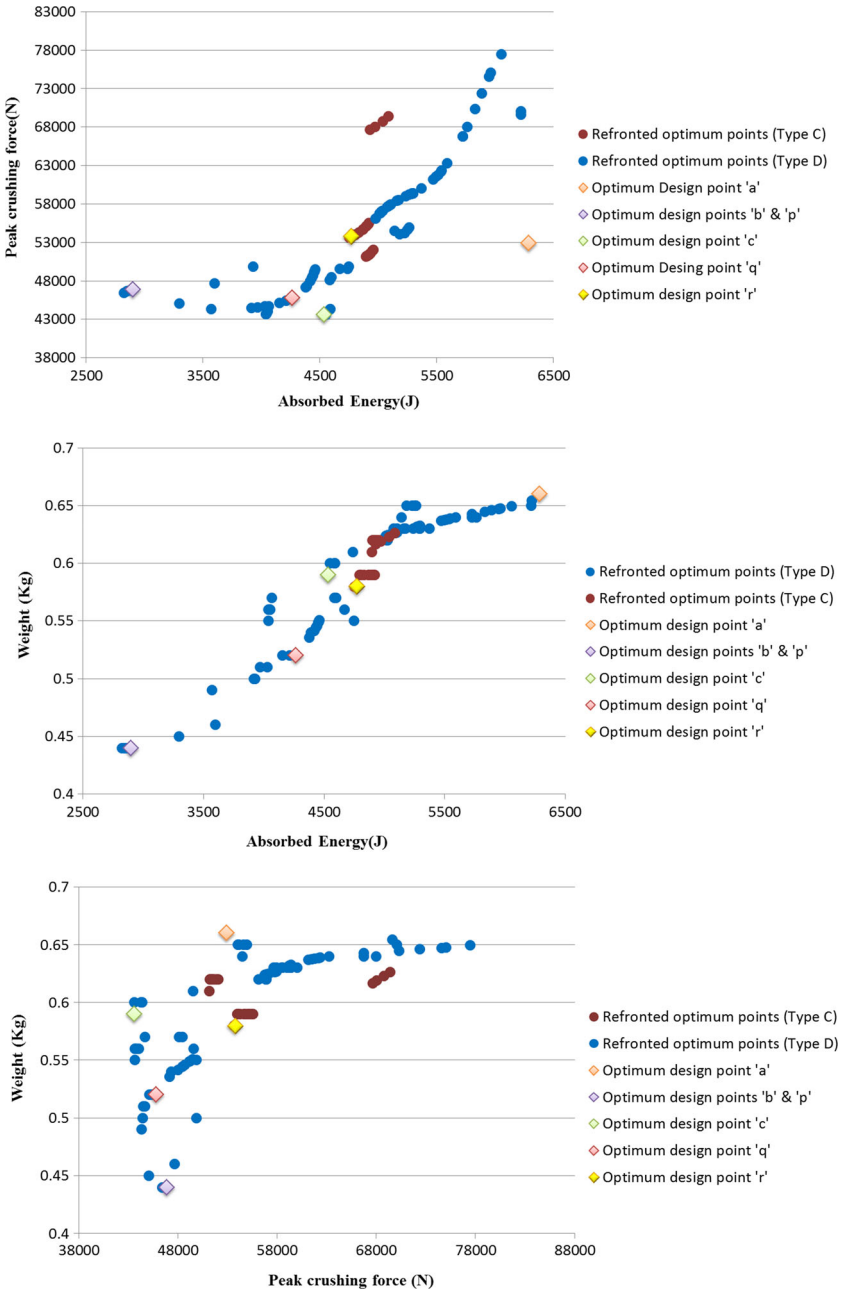

Fig. 12 The obtained optimum design points in different planes

that this point have moderate values for objective functions in comparison to other obtained optimum design points.

To show the accuracy of the optimum solutions, the trade-off optimum design points have been re-evaluated by the finite element method in a post numerical study. It should be noted that the trade-off optimum design points in both cases are not included in the training and testing sets which makes such re-evaluation sensible. The results of such FEM analysis re-evaluations are compared with those obtained from the optimization process in Table 7. The close agreement of such comparison demonstrates the effectiveness of the approach of this paper both in deriving the surrogate model and in obtaining the optimum solutions.

7 Conclusion

The crashworthiness characteristics of the thin-walled square tubes with geometrical discontinuities in the form of circular holes under quasi-static axial load were studied both experimentally and numerically. Static tests with 16 specimens were

Table 6 Values of design parameters and objective functions for the trade-off optimum design points altogether with the results of single objective optimizations

Optimum design points		*a*	*b*	*c*	*p*	*q*	*r*
Type		D	D	D	D	D	C
Number of holes on perforated sides (n)		1	3	1	3	3	2
Holes diameter		8.8	44.9	42.6	44.9	35	45.3
Energy abortion (J)		6286.67	2900.05	4536.41	2900.05	4264.29	4769.15
Peak crushing force (N)		52885.1	46853.1	43596.4	46853.1	45791.4	53765.4
Weight (Kg)		0.657	0.436	0.593	0.436	0.524	0.508
Comparison with the base line solution (%)	E	116 increase	–	56.4 increase	–	47 increase	64.4 increase
	F_{max}	12.8 increase	–	6.9 decrease	–	2.3 decrease	14.7 increase
	W	51 increase	–	36 increase	–	20 increase	16.5 increase

Table 7 Results of FEM analysis re-evaluations for the trade-off optimum design points and non-perforate tube

Design points		*a*	*b*	*C*	*P*	*q*	*r*	Non perforated
Energy abortion (J)	GMDH model	6286.67	2900.05	4536.41	2900.05	4264.29	4769.15	–
	FEM	5843.9	2972.2	4328.3	2972.2	4142.7	4431.9	5948.9
Peak crushing force (N)	GMDH model	52885.1	46853.1	43596.4	46853.1	45791.4	53765.4	–
	FEM	57194	46626	40891	46626	48155	53549	79310
Weight (Kg)		0.657	0.436	0.593	0.436	0.524	0.508	0.66

carried out to validate the finite element model performed using ABAQUS. Comparison between the load–displacement graphs, collapse modes, amount of the absorbed energies and peak crushing forces showed that the numerical results are in good agreement with the experimental data. GEvoM software was introduced and successfully employed to obtain polynomials for modeling the absorbed energy and peak crushing force based on 96 input–output data obtained from the FE simulations. Such polynomial models showed very good behavior in the test and train sets. To find the optimal configuration of holes on the perforated square tubes to achieve improved crashworthiness characteristics of the tubes under quasi static axial load, a multi-objective optimization problem was defined. The absorbed energy, peak crushing load and weight of the structure were considered as three conflicting objectives in the MOP. To solve this MOP the modified NSGAII and MOPSO were employed and the solutions were combined for non-dominated sorting to obtain the optimum points. 105 non-dominated optimum design points were extracted from solving the MOP. About 70 % of the non-dominated optimum points are from type D. This interesting result shows that square tubes with more perforated sides have better crashworthiness characteristics. To find the trade-off design point among the non-dominated optimum points, NIP and TOPSIS methods were applied. Optimum design points found from these two methods can be selected by designers as compromising optimum points confidently.

Appendix A

Corresponding polynomial representation for absorbed energy of types A, B, C and D obtained using GEvoM are as follows:

For Type A:

$$
\begin{aligned}
Y_1 &= 4849.3294 - 37.2842D + 0.42835D^2 \\
Y_2 &= 4922.798 - 543.668n + 91.682n^2 \\
Y_3 &= -0.0058 + 16.5079Y_1 - 16.629Y_2 - 0.000984Y_1^2 + 0.002858Y_2^2 - 0.001611_2Y_1 \\
Y_4 &= 0.000394 + 0.0055219D + 0.848535Y_2 + 0.3681567D^2 + 6.8241156Y_2^2 - 0.008267Y_2D \\
Energy &= 0.005755 - 24.66255Y_3 + 25.44598Y_4 + 0.01772Y_3^2 + 0.0119459Y_4^2 - 0.0296227\mathrm{Y_3Y_4}
\end{aligned}
\tag{4}
$$

For Type B:

$$
\begin{aligned}
Y_1 &= 4189.0752 - 195.03608n + 36.69127D + 83.207066n^2 - 0.34526D^2 - 14.05867nD \\
Y_2 &= 4321.49518 - 7.42745D - 0.02677D^2 \\
Y_3 &= -0.46187 - 91.45453D + 1.94702Y_1 + 0.10591D^2 - 0.00022{Y_1}^2 + 0.0205698DY_1 \\
Y_4 &= -0.003539 + 10.14823Y_1 - 8.94379Y_2 - 0.000487{Y_1}^2 + 0.0017609{Y_2}^2 - 0.001321Y_1Y_2 \\
Energy &= -0.03759 - 14.38065Y_3 + 15.49129Y_4 - 0.03292{Y_3}^2 - 0.03677{Y_4}^2 + 0.06967Y_3Y_4
\end{aligned}
\tag{5}
$$

For Type C:

$$
\begin{aligned}
Y_1 &= 5778.8423 - 811.9339n + 60.38783D + 142.6619n^2 - 1.38307D^2 - 5.90438892781643nD \\
Y_2 &= 4787.22183 + 39.71079D - 1.1467D^2 \\
Y_3 &= 5974.887 - 1188.5924n + 227.629n^2 \\
Y_4 &= -0.00215 + 5.2949Y_1 - 4.32067Y_2 - 0.000182{Y_1}^2 + 0.00075{Y_2}^2 - 0.000568Y_1Y_2 \\
Y_5 &= 4.579{*}10^{-5} + 0.986081Y_2 + 0.004101 + 2.8974{*}10^{-6}{Y_2}^2 \\
Y_5 &= 0.007725 - 0.421966n + 0.96043Y_2 + 105.5038n^2 + 5.60010{*}10^{-5}{Y_2}^2 - 0.15632nY_2 \\
Y_6 &= 0.000523 + 0.008127D + 1.2338Y_3 - 1.1458D^2 - 4.4885{*}10^{-5}Y32 + 0.008275DY_3 \\
Y_7 &= -0.00091 + 3.00512Y_4 - 1.87748Y_5 - 0.00035{Y_4}^2 + 0.0001{Y_5}^2 + 0.00023Y_4Y_5 \\
Y_8 &= 0.0025106 - 9.26457Y_5 + 10.43103Y_6 + 0.00177{Y_5}^2 - 0.00029{Y_6}^2 - 0.001524Y_5Y_6 \\
Energy &= -0.00504 + 8.22627Y_7 - 6.74763Y_8 + 0.00338{Y_7}^2 + 0.004716{Y_8}^2 - 0.008209Y_7Y_7
\end{aligned}
\tag{6}
$$

For Type D:

$$
\begin{aligned}
&Y_1 = 6860.736-980.45n-14.57D + 179.605n^2-0.1042D^2-10.9524nD \\
&Y_2 = 6051.591-1054.599n + 139.517n^2 \\
&Y_3 = 5931.642 + 56.764D + 0.44536D^2 \\
&Y_4 = 0.14737 + 0.9183Y_1 + 10.1842D + 1.4308Y_1{}^2-0.0636D^2-0.0013Y_1D \\
&Y_5 = -0.001627-6.610366Y_2 + 6.45366Y_3 + 0.00097Y_2{}^2-0.00044Y_3{}^2-0.000278Y_2Y_3 \\
&Y_6 = 9.6249 + 0.7868Y_1 + 0.21856Y_2-4.341*10^{-5}Y_1{}^2-9.0711*10^{-5}Y_2{}^2 + 0.0001338Y_1Y_2 \\
&Y_7 = 0.004549*10^{-5} + 9.6103Y_4-8.568Y_5 + 0.00247Y_4{}^2 + 0.00465Y_5{}^2-0.0071Y_4Y_6 \\
&Y_8 = 0.0024 + 11.954Y_7-10.825Y_5-0.001643Y_7{}^2 + 0.00106Y_6{}^2 + 0.000551Y_7Y_6 \\
&Energy = -0.04637-9.368Y_7-9.368Y_8 + 10.2556Y_7{}^2 + 0.05517Y_8{}^2 + 0.05395Y_7Y_8
\end{aligned}
\tag{7}
$$

Similarly, the corresponding GEvoM polynomial representations to model the peak crushing force of types A, B, C and D are in the form of:

For Type A:

$$
\begin{aligned}
&Y_1 = 71238.1224-870.4868n + 454.9678n^2 \\
&Y_2 = 84266.5655-2926.3874n + -376.9989D + 518.2299n^2-0.259431D^2 + 29.1475nD \\
&Y_3 = 1.3662*10^{-5} + 0.499Y_2 + 0.49771Y_1 + 1.16274*10^{-6}Y_2{}^2-5.7945*10^{-6}Y_1{}^2 + 4.668*10^{-6}Y_2Y_1 \\
&F_{max} = 1.38108*10^{-5} + 0.48753Y_3 + 0.48719Y_2 + 0.122235Y_3{}^2 + 0.122339Y_2{}^2-0.24457Y_3Y_2
\end{aligned}
\tag{8}
$$

For Type B:

$$
\begin{aligned}
&Y_1 = 85895.284-3899.7748n + -582.285D + 1253.2236n^2 + 4.76153D^2-125.8719nD \\
&Y_2 = 3.05887*10^{-5} + 1.00757Y_1 + 3.6393*10^{-5}n-1.00799*10^{-7}Y_1{}^2 + 2.24438*10^{-5}n^2-0.00032Y_1n \\
&F_{max} = 1.24071*10^{-5} + 0.5155Y_1 + 0.51372Y_2-0.16627Y_1{}^2-0.16633Y_2{}^2 + 0.33261Y_2Y_1
\end{aligned}
\tag{9}
$$

For Type C:

$$
\begin{aligned}
&Y_1 = 66993.5678-4235.856\,6n + 1348.3893n^2 \\
&Y_2 = 108903.8198-14710.046n-1185.1545D + 2066.7706n^2 + 3.29294D^2 + 131.38259nD \\
&Y_3 = 84253.48327-597.72D-1.352117D^2 \\
&Y_4 = 2.70313*10^{-4} + 1.00426Y_1-6.42003*10^{-8}Y_1{}^2 \\
&Y_5 = 1.58153*10^{-5} + 0.50779Y_2 + 0.5082Y_3 + 0.0004234Y_2{}^2 + 0.0004294Y_3{}^2-0.0008536Y_2Y_3 \\
&F_{max} = 9.97831*10^{-6} + 0.3374849Y_4 + 0.33079Y_5 + 2.156436*10^{-6}Y_4{}^2 + 7.03301Y_5{}^2-4.36705Y_4Y_5
\end{aligned}
\tag{10}
$$

For Type D:

$$
\begin{aligned}
&Y_1 = 99723.8754-9784.638n-1747.028D + 1608.228n^2 + 16.2803D^2 + 52.97698nD \\
&Y_2 = 61963.2877-2577.7168n + 310.175n^2 \\
&Y_3 = -1.50565*10^{-5} + 0.962219Y_1-0.00595D + 3.348628*10^{-7}Y_1{}^2-0.841921D^2 + 0.0012934Y_1D \\
&Y_4 = 1.3662*10^{-5} + 0.4074Y_1 + 0.39829Y_2-8.0952*10^{-6}Y_1{}^2-1.58136*10^{-5}Y_2{}^2 + 2.75687*10^{-5}Y_1Y_2 \\
&Y_5 = 1.3662*10^{-5} + 0.39831Y_2 + 0.40747Y_1-1.58138-05Y_2{}^2-8.0952*10^{-6}Y_1{}^2 + 2.75686*10^{-5}Y_2Y_1 \\
&Y_6 = 1.62774*10^{-5} + 0.49318Y_3 + 0.489156Y_4 + 0.004105Y_3{}^2 + 0.004102Y_4{}^2-0.008209Y_3Y_4 \\
&Y_7 = 1.68271*10^{-5} + 0.49943Y_5 + 0.50486Y_1 + 0.00382Y_5{}^2 + 0.0038Y_1{}^2-0.007657Y_5Y_1 \\
&F_{max} = 1.76673*10^{-5} + 0.532Y_6 + 0.531Y_7-0.00276Y_6{}^2-0.00276Y_7{}^2 + 0.005484Y_6Y_7
\end{aligned}
\tag{11}
$$

References

Amanifard N, Nariman-zadeh N, Borji M, Khalkhali A, Habibdoust A (2008a) Modelling and Pareto optimization of heat transfer and flow coefficients in microchannels using GMDH type neural networks and genetic algorithms. Int J Energy Convers Manag 49(2):311–325

Amanifard N, Nariman-Zadeh N, Farahani MH, Khalkhali A (2008b) Modelling of multiple short-length-scale stall cells in an axial compressor using evolved GMDH neural networks. Int J Energy Convers Manag 49(10):2588–2594

Arnold B, Altenh W (2004) Experimental observations on the crush characteristics of AA6061 T4 and T6 structural square tubes with and without circular discontinuities. Int J Crashworthiness 9(1):73–87

Arora JS (2012) Introduction to optimum design, Third Edition, Academic Press is an imprint of Elsevier

Atashkari K, Nariman-Zadeh N, Gölcü M, Khalkhali A, Jamali A (2007) Modelling and multi-objective optimization of a variable valve-timing spark-ignition engine using polynomial neural networks and evolutionary algorithms. Int J Energy Convers Manag 48(3): 1029–1041

Bartczak B, Gierczycka-zbrożek D, Gronostajski Z, Polak S, Tobota A (2010) The use of thin-walled sections for energy absorbing components: a review. Arch Civ Mech Eng 10(4):5–19

Chenga Q, Altenhofa W, Lib L (2006) Experimental investigations on the crush behaviour of AA6061-T6 aluminum square tubes with different types of through-hole discontinuities. Int J Thin Walled Struct 44:441–454

Clerc M, Kennedy J (2002) The particle swarm–explosion, stability, and convergence in a multidimensional complex space. IEEE Trans Evol Comput 6(1):58–73

Coello Coello CA, Christiansen AD (2000) Multiobjective optimization of trusses using genetic algorithms. Comput Struct 75:647–660

Coello Coello CA, Van Veldhuizen DA, Lamont GB (2002) Evolutionary algorithms for solving multi-objective problems. Kluwer Academic Publishers, NY

Coello CAC, Pulido GT, Lechuga MS (2004) Handling multiple objectives with particle swarm optimization. IEEE Trans Evol Comput 8(3):256–279

Collette Y, Siarry P (2003) Multiobjective optimization: principles and case studies. Decision engineering series. Springer, Berlin

Ebbesen S, Kiwitz P, Guzzella L (2012) A generic particle swarm optimization matlab function. American Control Conference Fairmont Queen Elizabeth, Montréal, Canada

Fonseca CM, Fleming PJ (1993) Genetic algorithms for multi-objective optimization: formulation, discussion and generalization. In: Forrest S (ed) Proceedings of the fifth international conference on genetic algorithms. Morgan Kaufmann, San Mateo, pp 416–423

Guoxing L, Tongxi Y (2003) Energy absorption of structures and materials. Woodhead Publishing Ltd and CRC Press LLC, England

Ivakhnenko AG (1971) Polynomial theory of complex systems. IEEE Trans Syst Man Cybern SMC-1:364–378

Johnson W (1972) Impact strength of material. London, Edward Arnold, 760 London, UK

Johnson W, Reid SR (1978) Metallic energy dissipating systems. Appl Mech Rev 31(3):277–288

Jones N, Wierzbicki T (1983) Structural crashworthiness. Butterworth and Co. Publishers, London

Kennedy J, Eberhart R (1995) Particle swarm optimization, in Neural Networks. IEEE Int Conf 4:1942–1948

Khakhali A, Darvizeh A, Masoumi A, Nariman-Zadeh N, Shiri A (2010) Robust design of S-shaped box beams subjected to compressive load, mathematical problems in engineering, Volume 2010. Article ID 627501, 18 p

Khakhali A, Nariman-zadeh N, Darvizeh A, Masoumi A, Notghi B (2010b) Reliability-based robust multi-objective crashworthiness optimisation of S-shaped box beams with parametric uncertainties. Int J Crashworthiness 15(4):443–456

Khakhali A, Darvizeh A, Masoumi A, Nariman-zadeh N (2011) Experimental and numerical investigation into the quasistatic crushing behaviour of the S-shape square tubes. J Mech 27(04): 585–596

Khalkhali A, Safikhani H (2011) Pareto based multi-objective optimization of cyclone vortex finder using CFD, GMDH type neural networks and genetic algorithms, engineering optimization, Volume 44, Issue 1, 2012

Khalkhali A, Farajpoor M, Safikhani H (2011) Modeling and multi-objective optimization of forward-curved blades centrifugal fans using CFD and neural networks. Trans Can Soc Mech Eng 35(1): 63–79

Liu GP, Kadirkamanathan V (1999) Multi-objective criteria for neural network structure selection and identification of nonlinear systems using genetic algorithms. IEE Proc Control Theory Appl 146(5): 373–382

Mamalis AG, Manolakos DE, Spentzas KN, Ioannidis MB, Koutroubakis S, Kostazos PK (2009) The effect of the implementation of circular holes as crush initiators to the crushing characteristics of mild steel square tubes: experimental and numerical simulation. Int J Crashworthiness 14(5):489–501

Nariman-Zadeh N, Darvizeh A, Jamali A (2006) Pareto optimization of energy absorption of square aluminum columns using multi-objective genetic algorithms. Proc Inst Mech Eng B J Eng Manuf 220(2):213–224

Pareto V (1896) Cours d'economic politique. Rouge: Lausanne, Switzerland

Shi Y, Eberhart RA (1998) modified particle swarm optimizer. In Proceedings of the IEEE International Conference on Evolutionary Computation, IEEE Press, Piscataway, p 69–73

Srinivas N, Deb K (1994) Multiobjective optimization using nondominated sorting in genetic algorithms. Evol Comput 2(3): 221–248

Tavoli A, Nariman-zadeh N, Khalkhali A, Mehran M (2006) Multi-objective optimization of abrasive flow machining processes using polynomial neural networks and genetic algorithms. Int J Mach Sci Technol 10(4):491–510